PHYSICAL REVIEW B VOLUME 43, NUMBER 14 15 MAY 1991-I

Measurement of the binding energy of kink-site atoms of metals and alloys

Jiang Liu and Chun-wu Wu
Department of Physics, Pennsylvania State University, University Park, Pennsylvania 16802

Tien T. Tsong*
Physics Institute, Academia Sinica, Nankang, Taipei, Republic of China
(Received 4 October 1990)

The binding energies of kink-site atoms of several metals and alloys have been measured from a kinetic-energy analysis of low-temperature field-evaporated ions using a high-resolution pulsed-laser time-of-flight atom-probe field ion microscope. Data are collected from atomically well-defined surfaces. The binding energies of metal atoms in kink sites obtained by this low-temperature and high-field method are found to agree with the cohesive energies of these metals, derived by thermodynamic methods, to -0.03 ± 0.19 eV. The binding energy of Co atoms in Pt_3Co alloys, either in ordered state or in disordered state, is 0.65 ± 0.17 eV higher than that in Co metal whereas the binding energy of Pt in the alloy is about 0.1 eV lower than that in Pt metal. We present details of the experimental method and indicate other problems which can be studied with this method.

I. INTRODUCTION

The binding energy, whether between two atoms in a molecule or between an adsorbed atom and the substrate or between an atom and the solid, is one of the most basic properties of the physical system which is closely related to the dynamics of the atomic bond formation.[1,2] In solid-state and surface science, the binding energy, or cohesion, has been one of the long-standing and fundamental topics of theoretical and experimental investigations.[3] A fundamental understanding of many surface phenomena requires a knowledge of how the binding energy of an atom is related to its atomic environment, or the general cohesive properties and the forces holding the atom to its site of adsorption. These phenomena include the surface reconstruction, the growth of islands and surface layers and eventually a crystal from the vapor phase or the liquid phase, adsorption and desorption, two-dimensional phase transition, and surface reactivity, etc.

A well-known method for finding the binding energy of surface atoms as well as adsorbed atoms is by a temperature programmed thermal desorption. The cohesive energy of a solid as well as the binding energy of surface atoms is measured as the heat of vaporization or, more precisely, the heat of sublimation extrapolated to the zero temperature. When a crystal is heated, surface atoms will start to migrate and the surface layer may also start to melt before surface atoms are thermally desorbed. Thus the binding energy derived by the temperature programmed thermal desorption method is not atomic site specific, and Taylor and Langmuir, pioneers of this method to surface studies, call this energy the thermal desorption energy instead of the binding energy. We report here a measurement of the binding energy of surface atoms using a low-temperature, field desorption and evaporation method. This method finds the binding energy of surface atoms from the kinetic energy of the field-desorbed ions. As field desorption and evaporation is carried out at a temperature well below the room temperature where surface atoms are immobile and the crystal structure remains intact, the binding energy derived for these atoms is atomic site specific. In low-temperature field evaporation, lattice atoms are field evaporated from kink sites at lattice steps. Here we report a measurement of binding energy of kink-site atoms of metals and alloys using a high-resolution kinetic-energy analysis of low-temperature field-evaporated ions.

II. PRINCIPLE OF THE METHOD

Field desorption refers to the removal of surface atoms, regardless of whether they are adsorbed atoms or lattice atoms, by an applied high electric field. Field desorption can occur even at cryogenic temperatures. Field evaporation is a special case of field desorption where atoms involved are lattice atoms. Field evaporation is an important physical process in atom-probe field ion microscopy with which a field emitter surface can be processed to become atomically smooth, thus a high-resolution field ion image of the surface can be formed by a uniform projection of field ions. Surface atoms and layers as well as bulk atoms and layers can be chemically analyzed by mass spectroscopy by field evaporating surface atoms gradually. From a theoretical point of view, there is little difference between field desorption and field evaporation. Theories of field desorption and evaporation are now fairly well developed,[4,5] but a discussion of these theories is beyond the scope of this paper. Using these theories, the activation energy of field desorption Q can be related to various parameters of the atoms as well as the surface. The physical meaning as well as accurate values of many of these parameters are still poorly known. Thus it is difficult to relate the ion energy distribution of desorbed ions to the binding energy of the desorbed atoms based on these theories. For such a purpose, it is much easier

to use a Born-Haber energy cycle of the field desorption process.

Let us consider first the binding energy of a kink-site atom at the surface. A kink-site atom has exactly one-half the coordination number of a bulk atom. Kink sites are also from where all the atoms in a crystal, except the last few atoms when the crystal becomes very, very small, can be removed from the surface with exactly the same atomic environment, thus requiring exactly the same energy for all the atoms in the crystal. The energy needed to remove a kink-site atom E_k, or the binding energy of a kink-site atom, is therefore by definition equal to the cohesive energy of the solid E_c.[1,6]

Now let us find out what is the minimum energy needed to remove a kink-site atom from the surface to free space in the form of an $n+$ charged ion in the absence of an applied electric field. To remove an atom from a kink site to vacuum, an energy corresponding to its binding energy E_k is needed. The atom is then ionized to the $n+$ charge state which requires an energy of $\sum_i^n I_i$, the total ionization energy of the atom. n electrons are returned to the surface at the Fermi level, thereby an energy of $n\phi$ is regained where ϕ is the work function of the surface. Since the atom, at the instant of its removal, carries a thermal energy (kinetic energy) Q, the minimum energy needed for this process is given by

$$\Delta E_c = E_k + \sum_i^n I_i - n\phi - Q \ . \tag{1}$$

This minimum energy ΔE_c will be called the critical ion energy deficit for a reason explained later in the paper. The minimum energy needed to remove an atom in an adsorption site to free space in the form of an $n+$ ion is also given by Eq. (1), except E_k should now be replaced by Λ, the binding energy of this surface atom in its site of adsorption.

In low-temperature field evaporation, a high electric field F is applied to the surface. The binding energy of the surface atom is changed from Λ to $[\Lambda(F)+\frac{1}{2}\alpha' F^2]$ where $\Lambda(F)\equiv\Lambda'$ represents the crystal binding of the surface atom in the presence of the applied field F and α' is the effective polarizability of the surface atom in its adsorption site. α' is expected to be quite different from the free atom polarizability as the surface atom is partially shielded from the applied field by the conduction electrons. The critical ion energy deficit, or the minimum ion energy deficit, in field evaporation, which is the energy deficiency from the full acceleration energy of the applied voltage neV for the most energetic ions emitted, can be figured out using a Born-Haber energy cycle shown in Fig. 1.[7] In this diagram the potential energy of the system, consisting of a surface atom and the surface, in each of the intermediate states in field evaporation is listed under the state diagram. The energy needed to transform the system from one state to another is simply the difference in the potential energy of the final state and that of the initial state. This needed energy is listed by the arrow connecting the two states. It is clear from this diagram, after considering the thermal energy Q the particle carries at the instant of field desorption, that the critical ion energy deficit is given by

$$\Delta E_c = [\Lambda(F)+\tfrac{1}{2}\alpha' F^2] + \sum_i^n I_i - n\phi - Q \ . \tag{2}$$

It is important to realize that this critical ion energy deficit, which is a consequence of the conservation of the energy of the system during the ion formation, is in fact independent of the detailed steps of ion formation, or independent of whether the ions are formed by direct field evaporation, or by post field ionization of field-evaporated singly charged ions.[8] In contrast, a calculation of the field strength needed for field evaporation to occur requires knowledge of the mechanism or detailed steps of ion formation.

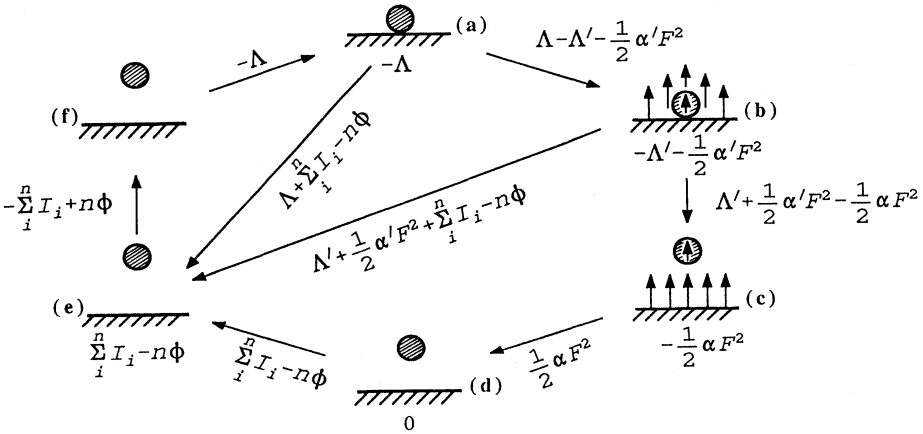

FIG. 1. A Born-Haber energy cycle showing the energetics in the low-temperature field desorption and evaporation process. Several intermediate states are shown. The potential energy of the system, which consists of the surface and an adatom, is listed below each state diagram. The energy needed to transform the system from one state to another is the difference in the potential energies of the final and the initial states.

Regardless of how $[\Lambda(F)+\frac{1}{2}\alpha' F^2]$ is dependent on the applied field, the asymptotic value of this quantity in zero field should be identical to the binding energy of the surface atoms in zero field, or $\lim_{F\to 0}[\Lambda(F)+\frac{1}{2}\alpha' F^2] = \Lambda(0)=\Lambda$. An important question is how large is the difference between $[\Lambda(F)+\frac{1}{2}\alpha' F^2]$ in the normal field-evaporation condition of the experiment and Λ. In the past, from a measurement of the field-evaporation rate as function of the applied field[9] and from a directional walk experiment,[10] it was concluded that the polarization binding energy of surface atoms, $\frac{1}{2}\alpha' F^2$, under the evaporation field can be as large as a few eV, or comparable to the crystal binding energy of the surface atoms Λ. It is the currently accepted view of most investigators in the field ion microscopy community that the crystal binding energy Λ is independent of the applied field, or $\Lambda(F)=\Lambda(0)=\Lambda$. Therefore $[\Lambda(F)+\frac{1}{2}\alpha' F^2]$ should be greater than Λ by as much as $\frac{1}{2}\alpha' F^2$. As our experimental data will show, such an assumption is a pure conjecture of physical intuitions. It lacks experimental substantiation. When a high positive electric field is applied, the binding energy of the surface atom is increased by the polarization energy $\frac{1}{2}\alpha' F^2$. However, the surface atom is also being denuded of the electronic charges responsible for the binding of the atom to the surface. Thus this increase in polarization binding is offset by a decrease in the crystal binding of the atom. As will be clear from further discussions, our result obtained with metals having evaporation fields in the range from 3.5 to 5.7 V/Å indicates that under these evaporation fields $[\Lambda(F)+\frac{1}{2}\alpha' F^2]$ and Λ are equal to one another, or independent of the applied field, to within the ± 0.2 eV accuracy of our measurement. It is therefore possible to measure the binding energy of surface atoms using an accurate, high-resolution kinetic-energy analysis of low-temperature field-evaporated ions without going through the tedious procedure of finding out how $[\Lambda(F)+\frac{1}{2}\alpha' F^2]$ is dependent on the field F and then taking the zero-field asymptotic value. This low-temperature high-field method simply measures very accurately the critical ion energy deficit from which the binding energy can be calculated according to

$$\Lambda \simeq [\Lambda(F)+\tfrac{1}{2}\alpha' F^2] = \Delta E_c + n\phi - \sum_i^n I_i + Q \ . \tag{3}$$

In low-temperature field evaporation, the activation energy Q is only about 0.1 to 0.2 eV especially at the very high field-evaporation rate of the pulsed-laser field evaporation, or about the same magnitude as the experimental uncertainty of this experiment.[11] Q will therefore be omitted in our data analysis.

Before we proceed to describe details of our experimental method, we would like to mention that a low-temperature field-evaporation method has been attempted earlier to determine the binding energy of adsorbed atoms.[12] This early method tries to relate the binding energy to their "evaporation field." Not only is the evaporation field a poorly defined quantity, it depends on the evaporation rate of the measurement and it can easily change over 15% when the evaporation is changed from dc voltage to the nanosecond pulsed-voltage field-evaporation rate. How this field is related to the binding energy is also poorly understood; it depends on the detailed steps in the theoretical model of field evaporation used, the charge state of the ions, and whether these ions are produced by post field ionization or not. Many of these questions are still unanswered. In contrast, the present method does not depend on the mechanisms of field evaporation. Equation (3) is derived from a Born-Haber energy cycle which does not depend on the detailed mechanisms of ion formation in field evaporation.

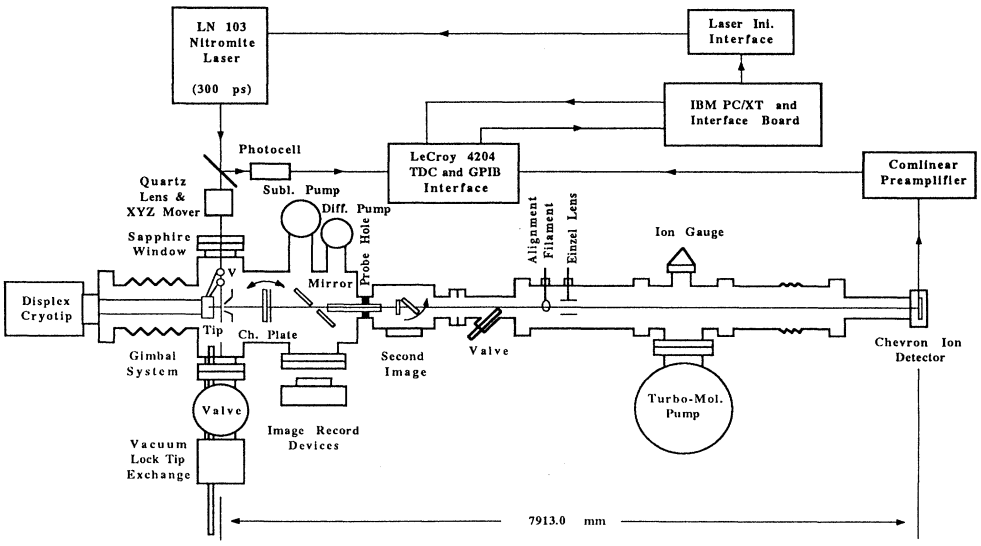

FIG. 2. The high-resolution pulsed-laser time-of-flight atom probe used in this study. Detailed description of this system can be found in the text. GPIB is a standard general purpose interface bus.

III. EXPERIMENTAL METHOD

A. Instrumentation

The instrument used in this experiment is a high-resolution pulsed-laser time-of-flight atom-probe field ion microscope.[13] A schematic of this instrument is shown in Fig. 2. The basic design of this system has been described earlier. In this experiment, we would want to achieve an accuracy of the binding energy measurement to ± a few %. Since the binding energy is on the order of a few eV, this requires an instrument precision of better than ±0.2 eV out of a total ion kinetic energy of 10 to 20 keV, or a precision of about 1 to 2 parts in 10^5. This atom probe is now equipped with two LeCroy 4204 time-digital converters (TDC's) of 156.25-ps time resolution for the ion flight time measurement. The preamplifier used for the Chevron-channel plate ion detector has a 1.1-GHz band-

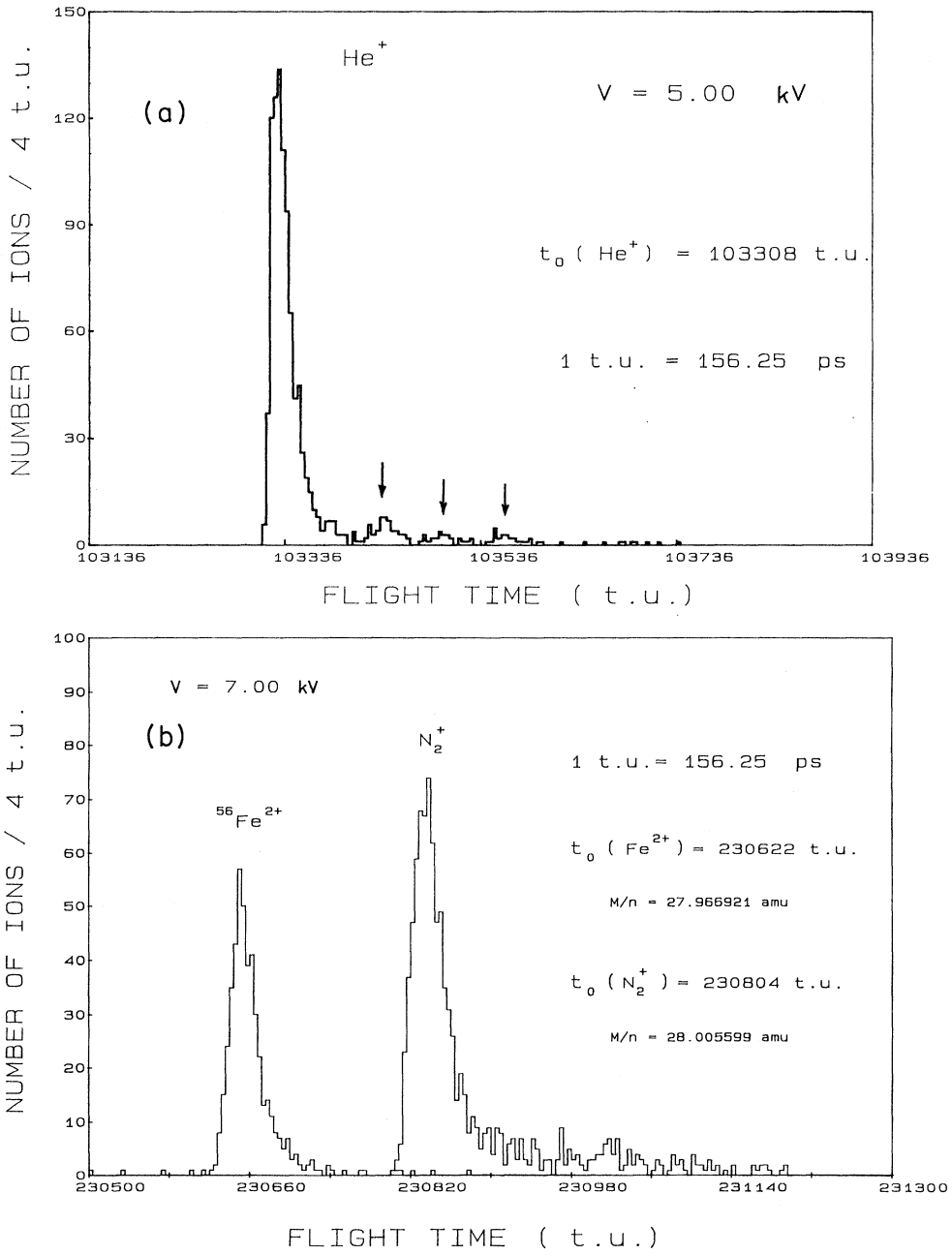

FIG. 3. (a) A time-of-flight spectrum, or an ion energy distribution of pulsed-laser field-desorbed He^+ ions taken at 5 kV. Note the resonance tunneling peaks similar to those found in ordinary field ionization. (b) Time-of-flight spectral lines of $^{56}Fe^{2+}$ and N_2^+ taken at 7.0 kV. These spectral lines are also high-resolution ion kinetic-energy distributions. Although these two ion species have the same mass-to-charge ratio, their onset flight times are separated by as many as 182 t.u.

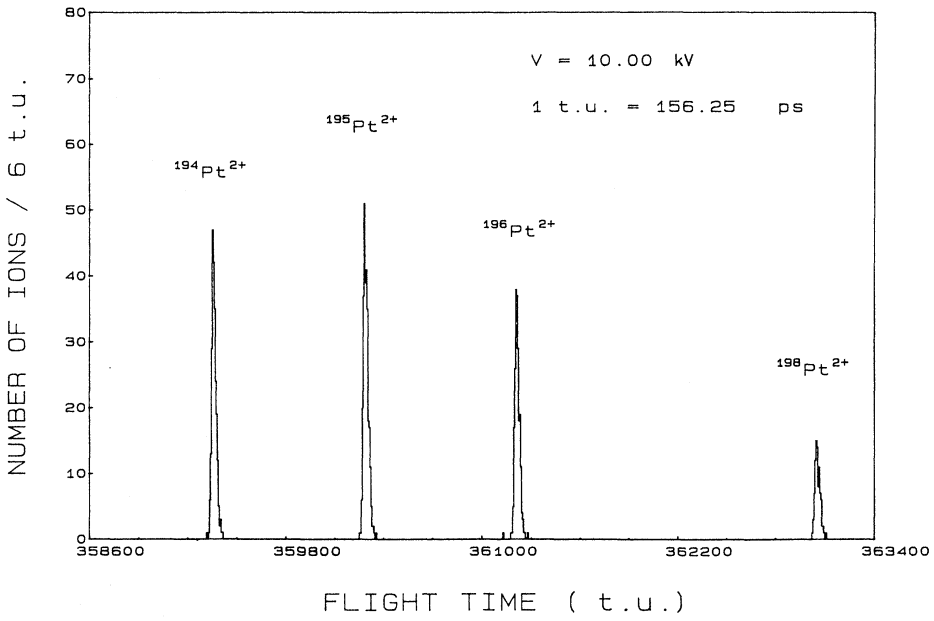

FIG. 4. A time-of-flight spectrum showing the four major isotopes of Pt. Each spectral line is also a high-resolution ion kinetic-energy distribution. Note the absence of noises in the spectrum, and the sharpness of these ion energy distributions. The full width at half maximum (FWHM) corresponds to an ionization zone of about 0.2 Å. There are no low-energy tails, indicating that these 2+ ions are unlikely to be produced by post field ionization (Ref. 8).

width and a 325-ps rise time. A dc power supply of 2 parts in 10^6 per hour stability is used for the tip voltage. The flight path is now extended to 7913.0 mm in length. The length determination is described in the next section. We also try to maintain the room temperature at ± 0.5 °C so that the flight path will not change more than ± 1 part in 10^5 by thermal expansion of the flight tube. The background pressure of the system is in the 1.5×10^{-9} to middle 10^{-10} Torr range. The surface is prepared by low-temperature, ~35 K, field evaporation. It is protected

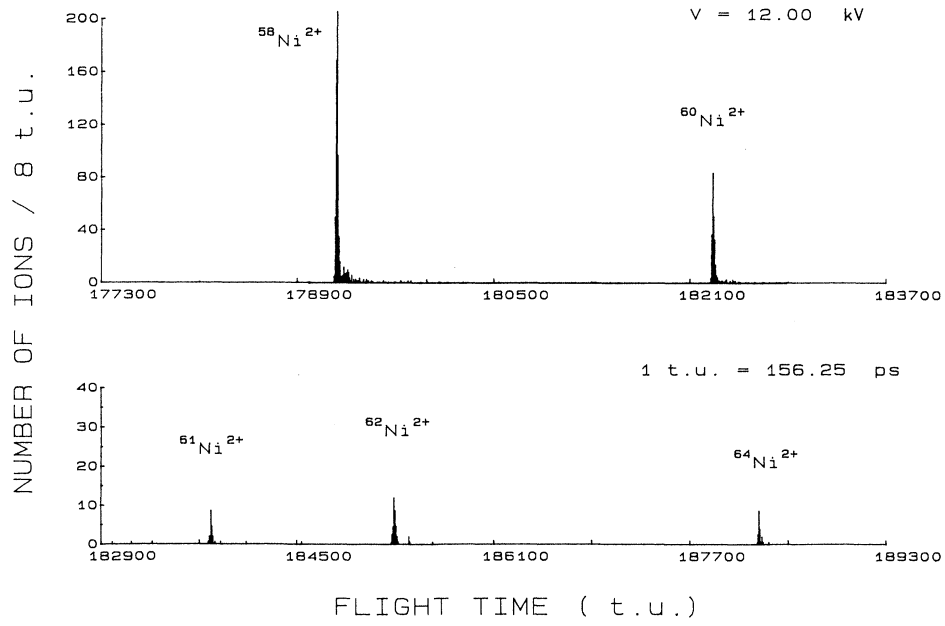

FIG. 5. A TOF spectrum for Ni taken at 12 kV. Very small low-energy tails can be seen. These low-energy ions are probably produced by post field ionization.

from a possible contamination of residual gases by the applied high electric field.

The ion flight times are recorded in a time unit (t.u.) of 156.25 ps, and the time-of-flight spectrum is plotted in a histogram of a desirable bin width. The bin width used is usually 2 to 6 t.u. for a high-resolution ion energy distribution, and over 8 t.u. for a mass spectrum. It is often necessary to collect well over 1000 ions for one ion energy distribution if a small bin width is used. The number of ions per bin should not be too small; otherwise the statistical uncertainty is too large. Figure 3(a) shows an ion energy distribution of pulsed-laser field-desorbed He^+ where resonance tunneling peaks can be seen. The system is capable of separating N_2^+ (28.005 599 u) from $^{56}Fe^{2+}$ (27.966 921 u) by 182 t.u. at the tip voltage of 7 kV as shown in Fig. 3(b). In Figs. 4 and 5 we show a time-of-flight mass and energy spectrum of Pt taken at 10 kV and one of Ni taken at 12 kV.

B. System calibration

To achieve the desired accuracy of ± 0.2 eV in the binding energy measurement, a very rigorous calibration of the system is needed even if the instrument precision is already sufficient.[14] In a high-resolution time-of-flight spectrometer, there are two system constants. These are the flight-path constant C and the time-delay constant δ. C is related to the flight-path length l according to $C=2e/l^2$, and δ accounts for the time delay of the system electronics and the signal traveling time in the connecting cables. If the two constants are known very accurately, then the critical ion energy deficit of any ion species can be calculated from its onset flight time in the ion energy distribution t_0, which is consistently taken to be at the 5% peak height of the high-energy side of the ion energy distribution, according to

$$\Delta E_c = ne\left[V_0 - \frac{M}{nC(t_0+\delta)^2}\right], \tag{4}$$

where M is the ionic mass (not atomic mass), and V_0 is the tip voltage. The ionic masses of elements are known from a standard table to an accuracy of better than 1 part in 10^6. On the other hand, it is impossible to measure the flight-path length and the delay time with good accuracy. Fortunately accurate values of C and δ can be obtained with a calibration method we have figured out earlier.[14] This method uses the onset flight times of pulsed-laser field-desorbed inert gas ions and molecular gas ions of known critical ion energy deficits to calibrate the system. The measured onset flight time t_0 is related to the system constants C and δ according to

$$t_0 = C^{-1/2}X - \delta\ . \tag{5}$$

where C is the flight-path constant, δ is the time-delay constant, and X is

$$X = \left[\frac{M}{n(V_0 - \Delta E_c/ne)}\right]^{1/2}. \tag{6}$$

Thus by measuring the onset flight times of various pulsed-laser field-desorbed gaseous species of known ΔE_c over a wide ionic mass range and a wide tip voltage range, and then plotting t_0 versus X using a linear-regression analysis, accurate values of C and δ can be obtained from the slope and the intercept of this linear plot. Table I lists data collected from 32 ion energy distributions of He^+, Ne^+, and N_2^+, and Ar^+ for the purpose of calibrating the system. In pulsed-laser stimulated field desorption of field-adsorbed (i.e., physical adsorption enhanced by the applied field) inert gases and molecular gases, gas atoms or molecules are thermally desorbed first and subsequently field ionized in the field ionization zone.[15] Their critical ion energy deficits are identical to those ions produced in ordinary field ionization. Experimental measurements of critical ion energy deficits in field ionization conclude that they are given by $(I-\phi)$, where I is the ionization energy of the gas and ϕ is the work function of the emitter surface.[16] In real measurements, because of a contact potential correction, the work function of the emitter surface has to be replaced by that of the collector in a retarding potential ion energy

TABLE I. Data for system calibration.

Ion species Ion mass (u)	$I-\phi$ (eV)	V_0 (kV)	t_0 (t.u.)
He^+	20.08	4.0	115 572
4.002 055		5.0	103 308
		5.5	98 478
		6.0	94 264
		7.0	87 246
		8.0	81 590
		9.0	76 908
		10.0	72 950
		10.5	71 184
		11.0	69 544
		12.0	66 572
Ne^+	17.06	5.0	230 936
19.991 890		5.5	220 156
		6.0	210 754
		7.0	195 074
		7.5	188 442
		8.0	182 440
		8.5	176 982
		9.0	171 982
		10.0	163 134
		11.0	155 524
		12.0	148 888
N_2^+	11.10	4.0	305 540
28.005 599		4.5	288 014
		5.0	273 198
		6.0	249 330
		7.0	230 804
Ar^+	11.23	4.5	344 062
		5.0	326 356
		6.0	297 866
		7.0	275 728
		7.5	266 360

Best fit parameters: $C=7.516\,220\,3\times10^{11}$ u/kV/(t.u.)^2, $\delta=94.7$ t.u.
Linearity: 0.999 999 998

TABLE II. Data for gaseous species.

Ion species	Ionic mass (u)	Calculated ΔE_c (eV)	Measured ΔE_c (eV)
He^+	4.002 055	20.08	20.10±0.18
Ne^+	19.991 890	17.06	17.00±0.19
N_2^+	28.005 599	11.10	11.14±0.13
Ar^+	39.961 834	11.23	11.29±0.16

analyzer. In a time-of-flight ion energy analyzer, it has to be replaced by the average work function of the flight tube as the ions spend most of their flight times in the flight tube. It is impossible to find out the average work function of the flight tube. We find that the linear plot has the best linearity if ϕ is taken to be 4.5 eV. The system constants derived from the linear-regression analysis are $C=7.516\,220\,3\times10^{11}\ u/\text{kV}/(\text{t.u.})^2$ and $\delta=94.7$ t.u. The linearity of the plot is 0.999 999 998, or it differs from the perfect linearity 1 by only 2×10^{-9}. From this value of the flight-path constant and $C=2e/l^2$, the flight-path length is calculated to be 7913.0 mm. Using these system constants, the critical ion energy deficit of any ion species can be calculated from its onset flight time using Eq. (4).

The system constants as well as the derived critical ion energy deficits will, of course, change slightly if one uses a different value of ϕ. However, we find that the binding energies derived from Eq. (3) are not sensitive to the value of ϕ used because they are compensated by this value of ϕ used at the right-hand side of Eq. (3) also. As long as ϕ is taken to have a value in the range from 4.9 to 4.1 eV, the binding energies derived will not shift more than 0.05 to 0.1 eV. Since the linearity of the calibration plot is the best when $\phi=4.5$ eV is used, we use this value for our data analysis. One may also worry about the voltage applied to the einzel lens. This question has already been answered in a detailed study.[13] It is found that as long as the voltage applied to the einzel lens is a constant fraction of the tip voltage, using a high-temperature stability and high-precision resistive voltage divider, the critical ion energy deficits derived will not change by more than 0.1 eV even though both the system constants and the onset flight times of the ion species will change considerably.

We can now, in reverse, calculate the critical ion energy deficits of the gaseous ion species listed in Table I using their onset flight times and the system constants. Table II shows the result. The measured values agree with theoretical values, $(I-\phi)$, to $+0.05\pm0.17$ eV. One may also use the theoretical critical ion energy deficits, the system constants, and the onset flight times to calculate the ionic masses. The ionic masses derived again agree to isotope masses to within one or two parts in 10^5. It is most gratifying to find that the overall consistency of the method is remarkable at the least and the reliability of the data presented is assured.

IV. EXPERIMENTAL RESULT AND DISCUSSIONS

A. Metals

In this first detailed experimental study of ours, we try to measure the binding energy of kink-site atoms of met-

TABLE III. Data for metals.

Ion species	M/n (u)	Measured $\Delta E_c/n$ (eV)	Measured E_k (eV)	Cohesive energy (eV)	Difference ΔE (eV)	Evaporation field (V/Å)
$^{56}Fe^{2+}$	27.966 921	9.77±0.08	4.50±0.16	4.32	+0.18±0.16	~3.5
$^{59}Co^{2+}$	29.466 050	10.13±0.04	4.34±0.08	4.41	−0.07±0.08	~3.6
$^{58}Ni^{2+}$	28.967 125	10.58±0.02	4.35±0.04	4.46	−0.11±0.04	~3.5
$^{60}Ni^{2+}$	29.964 846					
$^{103}Rh^{2+}$	51.452 477	10.97±0.09	5.41±0.17	5.78	−0.37±0.17	~4.8
		11.22±0.16	5.90±0.32	5.78	+0.12±0.32	
		11.23±0.16	5.92±0.16	5.78	+0.14±0.16	
$^{182}W^{3+}$	60.648 860					
$^{183}W^{3+}$	60.982 866	15.17±0.16	9.03±0.47	8.90	+0.13±0.47	~5.7
$^{184}W^{3+}$	61.316 436	15.12±0.17	8.88±0.51	8.90	−0.02±0.51	
$^{186}W^{3+}$	61.984 243					
$^{194}Pt^{2+}$	96.980 791					
$^{195}Pt^{2+}$	97.481 844	12.09±0.06	5.62±0.12	5.84	−0.22±0.12	~4.6
$^{196}Pt^{2+}$	97.981 925					
$^{198}Pt^{2+}$	98.983 391					
					−0.03±0.19 eV	

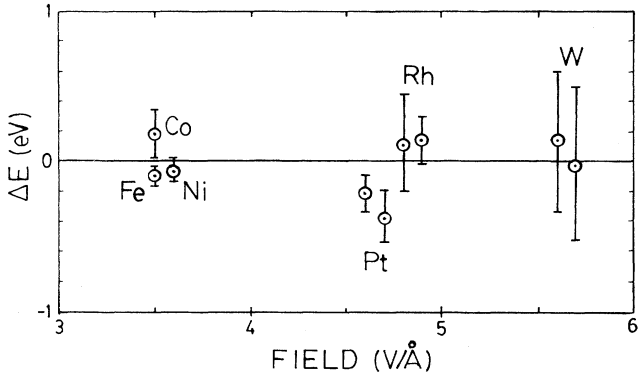

FIG. 6. Differences between the measured binding energies and the cohesive energies are plotted against the evaporation field of these metals. The fact that there is no apparent field dependence of these differences indicates that the binding energy measured by this method is independent of the applied field.

als for two reasons. First, in low-temperature field evaporation of metals, atoms are removed from kink sites one by one at the lattice steps. Thus it is experimentally much easier to measure the binding energy of kink-site atoms than that of atoms in other adsorption sites. Second, since the binding energy of kink-site atoms should be equal to the cohesive energy of the solid, this measurement can serve both to confirm the validity of the method and also the reliability of the existing data of the cohesive energy of solids. Once we are sure that our data are reliable, we then measure the binding energy of kink-site atoms of different atomic species in an alloy. This measurement serves two purposes. First, the binding energy of an atomic species should depend both on the atomic and the chemical environment of the atomic sites. We would like to be able to find out how the binding energy changes with the chemical environment. Second, as far as we are aware, no such data, the binding energies of consistent atoms of alloys in kink sites of the alloys, are available in the literature. Such data are essential for a fundamental understanding of atomic interactions in alloys and also of the formation of different alloy phases.

All the data reported here are taken in UHV with the tips cooled down to ~ 35 K. The minimum power of the laser is used for the stimulated pulsed field evaporation. The temperature reached by the pulsed-laser heating is estimated to be less than 150 K. Data are collected from the well-developed field-evaporated surface which has the (1×1) structure. The probe hole is aimed at the lattice steps of a low index plane where atoms are slowly field evaporated from their kink sites. The critical ion energy deficits obtained for five metals from this measurement and some data for rhodium and tungsten from a previous measurement[17] are listed in Table III.

The values of the measured binding energy E_k listed are really those of $[\Lambda(F)+\frac{1}{2}\alpha' F^2]$ at the evaporation fields. These fields are very different for different metals. The evaporation fields range from ~ 3.5 V/Å for Co and Fe to ~ 5.7 V/Å for W; these fields are estimated from the best image fields of image gases. Yet all these binding energies agree with the cohesive energies[18] of these metals to within -0.03 ± 0.19 eV. As shown in Fig. 6, neither is there any obvious field dependence of the difference between the measured binding energies $[\Lambda(F)+\frac{1}{2}\alpha' F^2]$ and the cohesive energies E_c. We therefore conclude the following: (1) Contrary to the general belief that the binding energy of surface atoms should be drastically changed by the applied electric field, our result shows that $[\Lambda(F)+\frac{1}{2}\alpha' F^2]$ differs from $\Lambda(0)$, or for kink-site atoms the cohesive energy of solid E_c, by -0.03 ± 0.19 eV, or less than the expected accuracy of our measurement which is about ± 0.2 eV. While this experimental finding is difficult to understand, and for many investigators difficult to believe, without going into detailed theoretical calculations, our qualitative explanation is that when a field is applied to the surface, the increase in the polarization binding $\frac{1}{2}\alpha' F^2$ is offset by an almost equal reduction in the crystal binding, or $[\Lambda(0)-\Lambda(F)]=\frac{1}{2}\alpha' F^2$. The reduction in the crystal binding can come from the denuding of binding electrons of the atom by the applied field. (2) It appears that values of cohesive energies listed in a standard table are reliable, at least they are consistent with our result. (3) Since the difference between $[\Lambda(F)+\frac{1}{2}\alpha' F^2]$ and $\Lambda(0)$ is less than ± 0.2 eV, this low-temperature field-evaporation method can be used for measuring the site-specific binding energy of surface atoms to this accuracy.

B. Alloys

An interesting problem for this first comprehensive study of ours is the energetics of alloy formation, particularly of ordered alloys. For an example, what are the binding energies of Co and Pt kink-site atoms in Pt_3Co and how do these energies compare with those in pure metals and also how do they change when the alloy is transformed from the disordered to the ordered state. Pt_3Co has a disordered fcc structure above 650 °C, and an ordered $L1_2$ fcc structure below 650 °C. Field ion micros-

TABLE IV. Data for Co, Pt, and Pt_3Co.

Ion species	Metal or alloy	Measured E_K (eV)	Cohesive energy (eV)
Co^{2+}	Co	4.34±0.08	4.41
Co^{2+}	Pt_3Co (disordered)	4.98±0.16	unknown
Co^{2+}	Pt_3Co (ordered)	5.00±0.17	unknown
Pt^{2+}	Pt	5.62±0.12	5.84
Pt^{2+}	Pt_3Co (ordered)	5.53±0.17	unknown

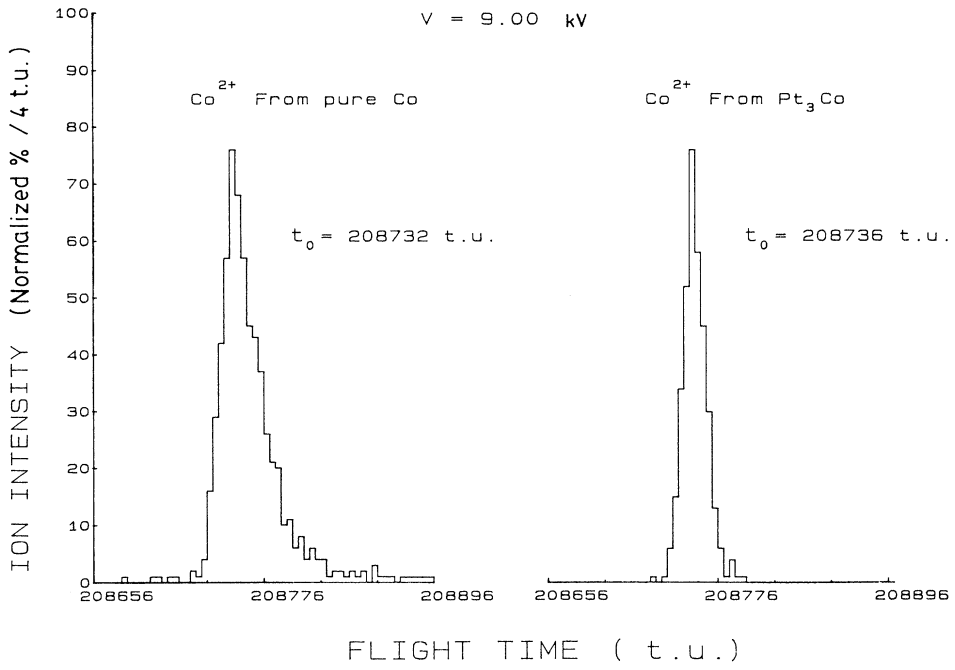

FIG. 7. Energy distributions of Co^{2+} ions in field evaporation of Pt_3Co alloy and Co metal. Note, not only the onset flight times are slightly different, the distribution widths are also different. The latter aspect is, however, beyond the scope of this paper.

copy (FIM) studies of Pt_3Co show that the disordered phase can be obtained by heating a tip above 650 °C and then be quenched.[19] The field ion image is very irregular. By annealing the tip *in situ* to around 600 °C for overnight, an ordered phase can be formed. The field ion image is very regular, showing only the symmetry of the Pt sublattice.

The pulsed-laser time-of-flight (TOF) atom-probe data obtained are listed in Table IV. The ion energy distribution of Co^{2+} ions from field evaporation of Pt_3Co has a slightly larger onset flight time than Co^{2+} ions from Co metal, see Fig. 7, indicating that Co atoms have a larger binding energy in Pt_3Co than in Co metal. In addition, the distribution widths for ions from these two different sources are quite different. However, this subject is beyond the scope of this paper. From these data we conclude the following: (1) Co atoms in Pt_3Co have a larger binding energy than in Co metal by 0.65 ± 0.17 eV whereas Pt atoms in Pt_3Co have a smaller binding energy than in pure Pt metal by 0.09 ± 0.18 eV. Since the binding energy gained by the Co atoms in this alloy is greater than that lost by the Pt atoms, this alloy should be stable with no phase separation, in agreement with known phase diagrams. (2) The difference in the binding energies of Co atoms in Pt_3Co in ordered and disordered phases is too small to be detected, or less than 0.2 eV, the accuracy of the present measurement. The binding energies of Co and Pt atoms in Pt_3Co should, of course, depend on the numbers of Co—Co, Co—Pt, and Pt—Pt bonds these atoms have in their sites of adsorption. At the present stage of the experimental development, however, we are unable to go into such a detailed analysis. Our present study gives only the average binding energies of Co and Pt kink-site atoms in a Pt_3Co alloy.

V. SUMMARY

The binding energies of kink-site atoms of several metals and an alloy have been measured using a low-temperature field-evaporation method. The binding energy of a surface atom in a field of 3.5 to 5.7 V/Å is found to be identical to the cohesive energy of the metal to within ±0.2 eV despite the fact that the polarization binding energy of a surface atom may be as large as a few eV. It appears that the polarization energy of the applied field is offset by the same amount due to a large reduction in the crystal binding of the atoms by the same applied field, probably due to a denuding of the bonding electronic charges by the field. Hence the binding energy of an atom on a metal or alloy surface is not dependent on the applied field. This conclusion is consistent with the experimental fact that there is no systematic deviation of the binding energies measured with this method from the cohesive energies of metals when the evaporation fields of these metals are changed from ~3.5 to ~5.7 V/Å from Co to W. In the future, it will be intersting to study the cohesion of atoms in compounds as well as the binding energy of adsorbed atoms on different adsorption sites of a surface or on different surfaces.

ACKNOWLEDGMENTS

This work was supported by the National Science Foundation, and in part supported by the National Science Council of the Republic of China through an award to T.T.T. We thank them for the support. We would also like to thank Mr. T.J. Eskew for his technical assistance.

---

*Author to whom inquiries should be directed. On leave from Physics Department, Pennsylvania State University, University Park, PA 16802..

[1]L. Pauling, Phys. Rev. **54**, 899 (1938); E. P. Wigner and F. Seitz, in *Solid State Physics* (Academic, New York, 1955), Vol. 1, p. 97; J. Bardeen and D. Pines, Phys. Rev. **99**, 1140 (1955); V. L. Muruzzi *et al.*, *Calculated Electronic Properties of Metals* (Pergamon, New York, 1978).

[2]G. W. Fernando, R. E. Watson, M. Weinert, Y. J. Wang, and J. W. Davenport, Phys. Rev. B **41**, 11 813 (1990).

[3]J. B. Taylor and I. Langmuir, Phys. Rev. **44**, 4236 (1933); see also J. T. Yates, in *Methods of Experimental Physics,* edited by R. Celortta and J. Levine (Academic, New York, 1985), Vol. 22, pp. 425–464.

[4]E. W. Müller, Phys. Rev. **102**, 618 (1956); R. Gomer and L. W. Swanson, J. Chem. Phys. **38**, 1613 (1963); E. R. McMullen and J. P. Perdew, Phys. Rev. B **36**, 2598 (1987); H. J. Kreuzer and K. Nath, Surf. Sci. **183**, 591 (1987).

[5]T. T. Tsong, Surf. Sci. Rep. **8**, 127 (1988); Rep. Prog. Phys. **51**, 759 (1988). Also see T. T. Tsong, *Atom-Probe Field Ion Microscopy* (Cambridge University Press, Cambridge, New York, 1990).

[6]M. P. Tosi, in *Solid State Physics,* edited by J. O. Hirschfelder (Interscience, New York, 1967), Vol. 16, p. 1.

[7]T. T. Tsong, Surf. Sci. **231**, 81 (1990).

[8]T. T. Tsong, Surf. Sci. **177**, 593 (1986).

[9]T. T. Tsong, J. Chem. Phys. **54**, 4205 (1971); R. G. Forbes, R. K. Biswas, and K. Chibane, Surf. Sci. **114**, 498 (1982).

[10]T. T. Tsong and G. L. Kellogg, Phys. Rev. B **12**, 1343 (1975); S. C. Wang and T. T. Tsong, *ibid.* **26**, 6470 (1982).

[11]See Ref. 5 and also G. L. Kellogg, Phys. Rev. B **29**, 4304 (1984).

[12]G. Ehrlich and C. F. Kirk, J. Chem. Phys. **48**, 1465 (1968); E. W. Plummer and T. N. Rhodin, *ibid.* **49**, 3474 (1969).

[13]T. T. Tsong, S. B. McLane, and T. J. Kinkus, Rev. Sci. Instrum. **53**, 1442 (1982). This instrument has been improved continuously by G. L. Hsao, Y. Liou, and the present authors.

[14]T. T. Tsong, Y. Liou, and S. B. McLane, Rev. Sci. Instrum. **55**, 1246 (1984); see also Ref. 5.

[15]T. T. Tsong, T. J. Kinkus, and S. B. McLane, J. Chem. Phys. **78**, 7497 (1983).

[16]A. J. Jason, Phys. Rev. **156**, 266 (1967); H. J. Heinen, F. W. Roellgen, and H. D. Beckey, Z. Naturforsch **29A**, 773 (1974); N. Ernst, G. Bozdech, and J. H. Block, Int. J. Mass Spectrom. Ion Phys. **28**, 33 (1978); see also Ref. 5.

[17]Y. Liou and T. T. Tsong, J. Phys. (Paris) Colloq. **49**, C6-105 (1988); J. Liu and T. T. Tsong (unpublished data).

[18]L. Brewer, Lawrence Berkeley Laboratory Report No. 3720 Rev. 1977 (unpublished); see C. Kittel, *Introduction to Solid State Physics,* 6th ed. (Wiley, New York 1986), p. 55.

[19]T. T. Tsong, and E. W. Müller, Appl. Phys. Lett. **9**, 7 (1966); J. Appl. Phys. **38**, 3531 (1967); H. N. Southworth and B. Ralph, Philos. Mag. **14**, 383 (1966).